Lab on a Chip

Accepted Manuscript

ROYAL SOCIETY OF CHEMISTRY

www.rsc.org/loc

Lab on a Chip

RSCPublishing

ARTICLE

On-chip cavity-enhanced absorption spectroscopy using a white light-emitting diode and polymer mirrors

Cite this: DOI: 10.1039/xoxxoooooox

Received ooth January 2012,
Accepted ooth January 2012

DOI: 10.1039/xoxxoooooox

www.rsc.org/

Cathy M. Rushworth,[a] Gareth Jones,[a] Martin Fischlechner, [b,d] Emma Walton,[c] and Hywel Morgan[a]

We have developed a disposable microfluidic chip with integrated cavity mirrors comprised of two pieces of 3M Vikuiti™ enhanced specular reflector II (ESRII) film, for performing cavity-enhanced absorption spectroscopy with a white light-emitting diode (LED). Compared to measurements made with a chip without cavity mirrors, the absorption path length is enhanced by a maximum factor of 28 at 544 nm, and the sensitivity is enhanced by approximately 5 times, enabling micromolar range detection limits to be achieved in an optical path length of only 50 µm.

1. Introduction

Microfluidic devices offer many advantages, including small footprint, low power and low reagent consumption, but sensitive detection in small volumes remains a challenge. Absorption spectroscopy is a popular detection technique, which is described by the well-known Beer-Lambert law:

$$A = -\log_{10}\frac{I}{I_0} = \varepsilon C l \qquad (1)$$

where A is the (decadic) absorbance, I is the transmitted light intensity, I_0 is the initial light intensity, ε is the (decadic) molar absorption coefficient, C is the concentration and l is the optical path length. While bench-top UV/vis spectrometers, in combination with 1 cm path length cuvettes, may achieve absorbance sensitivities around 10^{-3} absorbance units (a. u.), detection limits on-chip are often hampered by the significantly shorter path length. However, absorption measurements can be made in short path-length devices. For example, Srinivasan and coworkers placed a green LED and photodiode around a conventional electro-wetting on dielectric chip, reporting a minimum absorption change of 3.17×10^{-3} a. u. (at 545 nm) in an absorption path length of 475 µm.[1] Alternatively, optical fibres may be integrated in-plane around a microchannel. For example, Wu and coworkers integrated two optical fibres (62.5 µm core diameter) around a channel with an optimised absorption path length of 250 µm, detecting 50 mg/L lactate at 540 nm via an enzymatic assay.[2]

Efforts have also been made to increase the optical path length by collecting light that has travelled along the direction of liquid flow in the channel, enabling path lengths of a few centimetres to be obtained. For example, Sieben and coworkers integrated a green LED (525 nm peak emission) and photodiode around a 300 µm by 300 µm channel, resulting in a 25 mm absorption path length, achieving $A_{min} = 1.4 \times 10^{-3}$ a. u. at 525 nm.[3]

In a following paper, Floquet and coworkers used a similar microfluidic chip with integrated LED and photodiode obtaining $A_{min} = 2.2 \times 10^{-4}$ a. u. at 435 nm in a 700 µm by 400 µm channel with 80 mm absorption path length and 10 s signal averaging.[4] However, these long optical path length approaches requires careful minimisation of scattered light, achieved in the previous references through the use of black PMMA as an optically absorbing chip material.

Recently, there has been interest in applying a now well-established gas-phase method, termed cavity-enhanced absorption spectroscopy (CEAS), to the liquid-phase.[5, 6] In this method, the absorption is enhanced by placing the sample between two high reflectivity mirrors, thus increasing the probed volume without increasing the sample volume. For relatively small round-trip losses (< 25%), it has been shown that the absorbance can be approximated using[7]

$$2.3026A = 2.3026\,\varepsilon C l = \left(\frac{I_0}{I} - 1\right)(1 - R) \qquad (2)$$

where R is the total round-trip reflectivity, which would typically be the average of the mirror reflectivity, but will be lowered further by introducing additional surfaces and/or liquid within the cavity. Cavity-enhanced data can be compared directly to single-pass data, by defining the cavity-enhancement

factor (CEF) as $(1 - R)^{-1}$. For example, if R = 99%, then a CEF of 100 can be achieved.

This multi-pass approach makes cavity-based absorption techniques attractive for increasing on-chip path lengths. Most previously reported strategies involve the insertion of absorption cells between two cavity mirrors, shown schematically in Fig. 1(a). Of perhaps greatest relevance to this work, Neil et al. placed a microfluidic chip within a cavity formed from two highly reflective (R > 99.85%, 400 – 800 nm) broadband mirrors, using a supercontinuum source with a high sensitivity spectrometer.[8] The minimum detectable absorbance per pass was found to be $A_{min} = 1.8 \times 10^{-4}$ a. u., with a cavity-enhancement factor of 102. The optical path length through the chip was 320 µm, with a channel height of 1 mm, probed with a beam diameter of around 600 µm, providing an interrogated volume of around 90 nL.

A major limitation of liquid-phase CEAS experiments to date lies in the relatively high degree of experimental complexity and associated cost, in particular the requirement for expensive inorganic dielectric mirrors and typically a laser light source. In addition, the requirement for high optical quality surfaces intra-cavity, and precise alignment has arguably not yet been overcome for carrying out robust *in situ* liquid-phase measurements.

We are therefore interested in miniaturising the bench-top liquid-phase cavity system such as that used by Neil and coworkers[8] (and typified in Fig. 1(a)), by replacing the supercontinuum light source with a white LED and integrating low-cost, robust mirrors within the chip itself. This approach is shown schematically in Fig. 1(b).

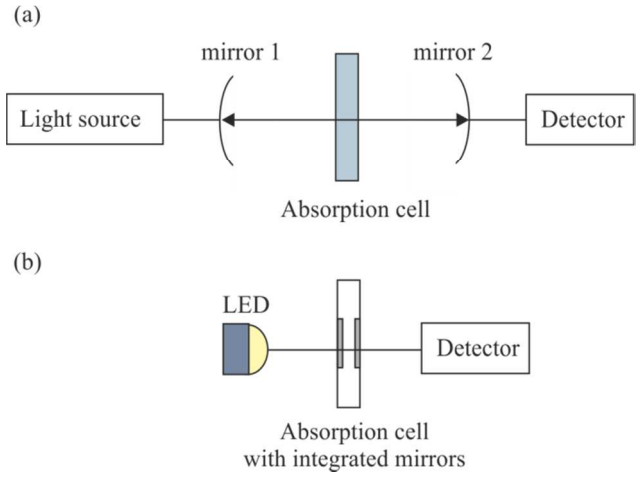

Fig. 1 (a) Schematic of bench-top liquid-phase cavity-enhanced absorption spectrometer. (b) Schematic of miniaturised set-up with integrated cavity mirrors.

Previous work has already demonstrated the potential for the use of LEDs with gas-phase[9] and liquid-phase cavity measurements.[10-12] Van der Sneppen and coworkers directly compared the results for a white LED to a supercontinuum source with evanescent-wave CEAS, examining three different mirror reflectivities (99%, 99.45%, 99.9%).[13] The authors reported that sensitivity with the LED was highest with the lowest reflectivity mirrors (99%), while the sensitivity with the supercontinuum source was highest with the highest reflectivity mirrors (99.9%), which they attributed to the lower power from the LED, and potential issues with LED/cavity alignment.

Two recent papers have demonstrated integration of metallic mirrors into microdevices to form a cavity, in the first instance for enhancing absorption measurements,[14] and in the second instance, for creating a droplet dye laser.[15] Billot and coworkers deposited 100 nm gold on either side of a 50 µm height polydimethylsiloxane (PDMS) channel, enabling the absorbance to be increased by a factor of 5. The poorer reflectivity of metallic mirrors compared with dielectric stack mirrors restricts the achievable CEFs, and there may also be a concern over the long-term stability of this approach, as the mirrors are in direct contact with the solution.

In this paper, we report for the first time the integration of 3M Vikuiti™ enhanced specular reflector II (ESRII) film within a microfluidic chip to form a cavity. ESRII film is a 32 µm thick multi-layer polyester film widely used in displays, and exhibits > 98% reflectivity across the entire visible spectrum.[16] In our chip design, the ESRII film is embedded within the PDMS layer, so that it does not come into contact with the liquid sample.

ESRII film has several distinct advantages over inorganic dielectric mirrors. Most importantly, because it is mass-produced, it is low-cost and can therefore be included in disposable microdevices, unlike more expensive inorganic dielectric mirrors. Secondly, as it is a thin film, it can easily be integrated into a microdevice as part of standard chip fabrication techniques. Thirdly, as ESRII film is a broadband reflector, it can be used in combination with a white LED to form a cavity suitable for measuring any visible-light absorbing species, making this a generic set-up. Finally, as will be seen, ESRII film forms a robust cavity which can be used to enhance the sensitivity of an absorption measurement by an order of magnitude without increasing the complexity of the optical system.

2. Experimental

2.1 Master Fabrication

The SU-8 master was fabricated using conventional rapid-prototyping techniques in a Class 1000 cleanroom, described more fully in the Supplementary Information. The resultant channel was 4 cm long and 500 µm wide, with one inlet and one outlet. Surface profile measurements (KLA Tencor, Alpha-Step) of the master indicated that the channel height was 47.3

μm ± 0.33 (three standard deviation error). The channel had a total filled volume of approximately 1 μL.

2.2 PDMS Chip Fabrication with ESRII film

Preparation of the PDMS and master is described in detail in the Supplementary Information. A 100 μm thick PDMS layer was obtained by spinning PDMS onto the master and a piece of 200 μm thick glass (Schott, D263 T eco) at 800 rpm for 30 seconds (Electronic Micro Systems Ltd., Model 4000). ESRII film was placed mirror-side face-down onto the PDMS layer on the master, and mirror-side face-up on the 200 μm thick unpatterned glass, after 10 minutes of baking at 100 ºC, once the PDMS was judged to be sufficiently immobile to allow for secure placement of the ESRII film, but tacky enough to adhere directly to the ESRII film without potentially trapping any air bubbles between the PDMS and the film. The PDMS was baked for a further 50 minutes. To facilitate the insertion of connectors into the channel, additional PDMS was poured over the master to a depth of a few millimetres and baked for 1 hour.

The PDMS was peeled carefully off the master and 1 mm fluid access holes were punched. The two halves of the microfluidic chip were placed face-up in an oxygen plasma asher (Diener Electronic GmbH, FEMTO) and oxidised for 30 seconds, before pressing both sides firmly together and baking at 80 ºC for 15 minutes. Using relatively large pieces of ESRII film aided quick alignment of the two halves of the chip.

A schematic of the microfluidic chip is shown in Fig. 2, along with a photo of the final device. The cavity length, defined by the distance between the two faces of the ESRII film, was estimated to be 200 μm.

2.3 Chemicals

All chemicals were purchased from Sigma-Aldrich and used without any further purification. Thymol blue indicator dye was chosen as an absorption standard as it absorbs across the entire visible spectrum, was found to be stable for several weeks, and does not adsorb to PDMS or glass. Thymol blue has also been well characterised in the literature as a pH indicator dye suitable for in situ spectrophotometric measurements of seawater pH.[17,18] A 2 mM stock solution of thymol blue sodium salt (Sigma-Aldrich, 861367-5G) was prepared in deionised water (MilliQ, Q-Pod, 0.22 μm filter, 18.2 MΩ.cm at 25 °C). 50 mM Tris buffer, nominally pH 8.8, was prepared by mixing 5.13 g Trizma base (Sigma-Aldrich, T1503-100G) and 1.23 g Trizma hydrochloride (Sigma-Aldrich, T3253-100G) in 1 L deionised water. The pH was measured as 9.0 ± 0.2 using two independent pH meters (Hanna Instruments, Checker1). The same buffer solution was used for all experiments. Thymol blue dye solutions were prepared in Tris buffer fresh daily. For concentrations > 100 μM, thymol blue was dissolved directly in Tris buffer.

2.4 Optical Measurements

A Luxeon Rebel ES cool white LED (RS, 733-6599), rated to produce a minimum of 200 lumens with a 700 mA driving current, was soldered to a heat pad (RS, 752-4982) and controlled with a constant current LED driver (Thorlabs, LEDD1B). The LED was secured to a two-adjuster mirror mount (Thorlabs, KM100). An optical fibre, with 300 μm core diameter (Ocean Optics, P300-1-SR) was mounted on a 3-axis translation stage (Newport, M-562), and delivered light to a spectrometer (Ocean Optics, HR4000CG-UV-NIR). The spectrometer collects light between 200 and 1100 nm with a resolution of 0.26 nm.

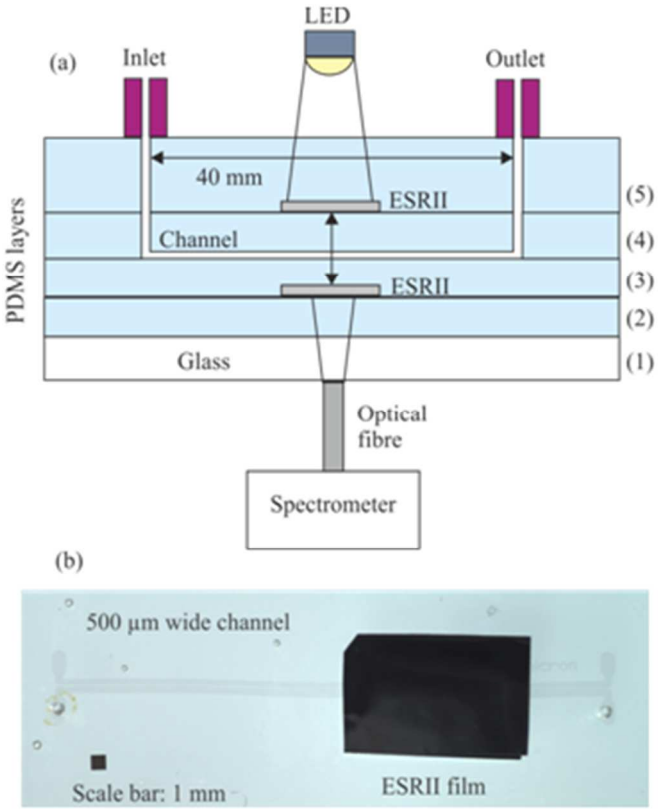

Fig. 2 (a) Side-view schematic (not to scale) of the microfluidic chip, showing the layers (1) to (5), which are as follows (all dimensions given are vertical): (1) 200 μm glass, (2) 100 μm PDMS (spun), (3) 32 μm ESRII film embedded in 100 μm PDMS (spun), (4) 50 μm channel embedded in 100 μm PDMS (spun) and (5) 32 μm ESRII film embedded in few mm PDMS (poured). (b) Photograph of microfluidic chip, with ESRII film.

The light intensity collected by the optical fibre was optimised before inserting the chip on a platform attached to a second 3-axis translation stage. By placing the 300 μm core diameter optical fibre (numerical aperture 0.22) as close as possible (approximately 300 μm) to the bottom of the cavity (Fig. 2), we ensured that only light that had been trapped within the ESRII film cavity within the channel region was collected by the spectrometer. In contrast, the LED illuminated a larger area than the channel. The probed volume, defined by the

characteristics and positioning of the optical fibre, was estimated to be 10 nL. It could be further reduced by using an optical fiber with smaller core diameter, at the potential expense of reducing the light intensity delivered to the spectrometer.

Fluid was pumped through the channel using a syringe pump operating at 0.5 mL/min. Approximately 20 seconds was found to be sufficient to flush the inlet tubing and channel thoroughly between each measurement, equivalent to approximately 170 µL sample volume per measurement, although the tubing/channel length was not optimised during this work. Absorbance spectra were acquired on static samples, although no significant difference was observed in the signal level or noise when acquired during flow.

The recorded I_0 values for the chip without and with ESRII film are presented in Fig. 3. The peaks of the white LED are well-matched to monitoring the absorbance of thymol blue at its acidic peak (435 nm) and its basic peak (595 nm).[17]

Although the signal intensities cannot be directly compared, as they were acquired at different LED drive currents (150 mA without ESRII film and 700 mA with ESRII film) and spectrometer integration times (50 ms without ESRII film and 1000 ms with ESRII film), Fig. 3 does provide a clear indication of the real signal levels at which absorbance data were acquired with and without ESRII film.

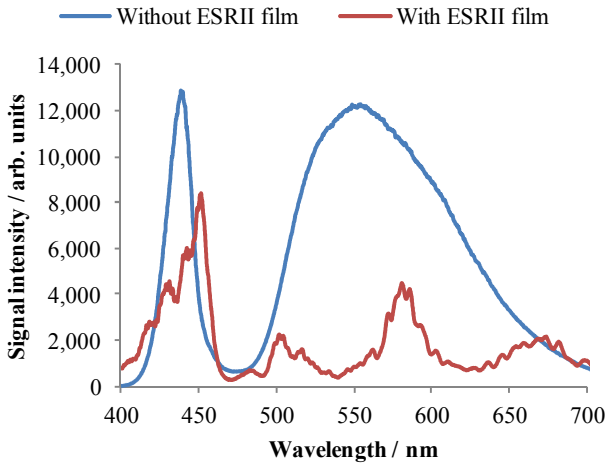

Fig. 3 Examples of the initial light intensity for channel filled with buffer only, without ESRII film (blue line) and with ESRII film (red line) demonstrating the modification of the white LED spectral output on passing through two pieces of ESRII film.

Data were recorded and analysed using a custom LabVIEW program. For each concentration, three pairs of I_0/I values were recorded, in order to assess the repeatability of the measurement, and to ensure complete washing of the channel between measurements, by monitoring the stability of I_0. Each spectrum recorded for either I_0 or I was the average of 10 acquired spectra, equivalent to an averaging time of 0.5 s for the chip without ESRII film and 10 s for the chip with ESRII film. To enable direct comparison of each set-up, the reported sensitivities have been normalised to 1 s acquisition.

The sensitivity of each optical set-up can be described in two ways.[11] Firstly, the sensitivity can be established from three times the standard deviation (3σ) in repeated measurements of I_0. This is referred to as the 'spectral' method, with detection limits given the subscript 's'. The second method establishes the sensitivity from the uncertainty in the y-intercept of a plot of the absorbance per unit path length (α) versus concentration, and is referred to as the 'regression' method, with detection limits given the subscript 'r'. Detection limits determined using the spectral method are typically lower than detection limits calculated using the regression method, as the spectral method includes only the inherent noise in the measurement (thus, representing the 'best-case' detection limit), while the regression method also includes uncertainties arising from concentration errors and cuvette/chip misalignments.

3. Results and Discussion

3.1 Bench-top UV/vis spectrometer measurements

The absorbance of six different concentrations of thymol blue indicator dye in the range 0.2 – 200 µM was first determined in 1 cm path length disposable plastic cuvettes using a bench-top spectrometer (PerkinElmer, Lambda 650). Data are presented in the Supplementary Information, Fig. S 1. In order to determine the spectral detection limit, ten repeated acquisitions of I_0 (Tris buffer) were acquired. The sensitivity using the regression method was assessed at the two peaks of the indicator dye, 435 nm and 595 nm. Data from the Supplementary Information are summarised in Table 1.

	435 nm	**595 nm**
$A_{min,s}$ / a. u.	2.73×10^{-4}	1.63×10^{-4}
$A_{min,r}$ / a. u.	1.34×10^{-2}	2.56×10^{-2}
ε / M^{-1} cm^{-1}	8910 ± 142	13,600 ± 272
$C_{min,s}$ / µM	0.031	0.020
$C_{min,r}$ / µM	1.50	1.89

Table 1 Summary of bench-top UV/vis spectrometer data. 3σ errors are provided for the absorption coefficient, ε.

The detection limits determined using the spectral method are approximately two orders of magnitude lower than the detection limits determined using the regression method. This indicates that the inherent noise within the spectrometer is significantly lower than the total experimental errors associated with, for example, positioning different cuvettes within the spectrometer.

3.2 Single-pass absorbance measurements on-chip

The absorbance of seven different concentration of thymol blue indicator dye in the range 50 – 2000 µM was measured on-chip, across the 50 µm height channel, without ESRII film.

A LED drive current of 150 mA was used in combination with a spectrometer integration time of 50 ms. Data are presented in Fig. 4. Good agreement was obtained between the absorbance spectra recorded on-chip and those determined using the bench-top spectrometer (Fig. S 1). Notice that the increased noise observed at 400 nm in Fig. 4 arises from the low light intensity from the white LED in this wavelength region (Fig. 3).

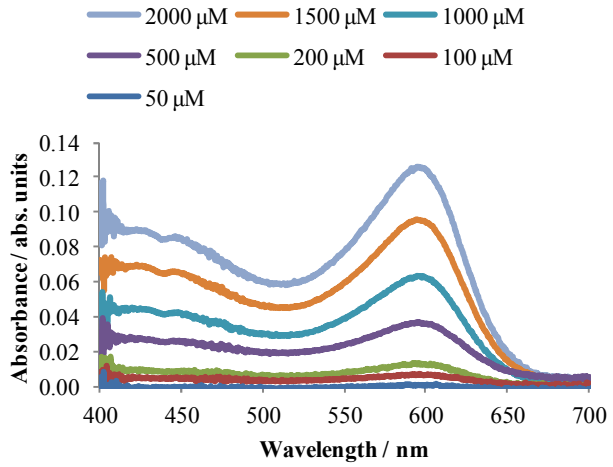

Fig. 4 Single-pass absorbance spectra of various concentrations of thymol blue, recorded through 50 µm height channel. The average of three pairs of recorded I_0/I values is shown for each concentration.

As an example, absorbance data for a range of concentrations at the dye peaks of 435 nm and 595 nm were extracted from Fig. 4 and are presented in Fig. 5. Good linearity was observed at both wavelengths, with $R^2 = 0.9860$ at 435 nm and $R^2 = 0.9923$ at 595 nm. The on-chip detection limit, in the absence of ESRII film, was determined from 3σ in 50 repeated measurements of I_0 (Tris buffer) to be $A_{min} = 9.38 \times 10^{-3}$ a. u. at 595 nm and $A_{min} = 1.03 \times 10^{-2}$ a. u. at 435 nm. The on-chip detection limits are summarised in Table 2.

	435 nm	595 nm
$A_{min,s}$ / a. u.	1.03×10^{-2}	9.38×10^{-3}
$A_{min,r}$ / a. u.	3.72×10^{-3}	4.00×10^{-3}
$\alpha_{min,s}$ / cm^{-1} Hz$^{-1/2}$	4.90×10^{-1}	4.46×10^{-1}
$\alpha_{min,r}$ / cm^{-1} Hz$^{-1/2}$	0.56	0.60
ε / M^{-1} cm^{-1}	9,300 ± 762	13,500 ± 819
$C_{min,s}$ / µM Hz$^{-1/2}$	52.7	33.1
$C_{min,r}$ / µM Hz$^{-1/2}$	60.1	44.6

Table 2 Detection limits determined on-chip, in the absence of ESRII film. 3σ errors are provided for the absorption coefficient, ε.

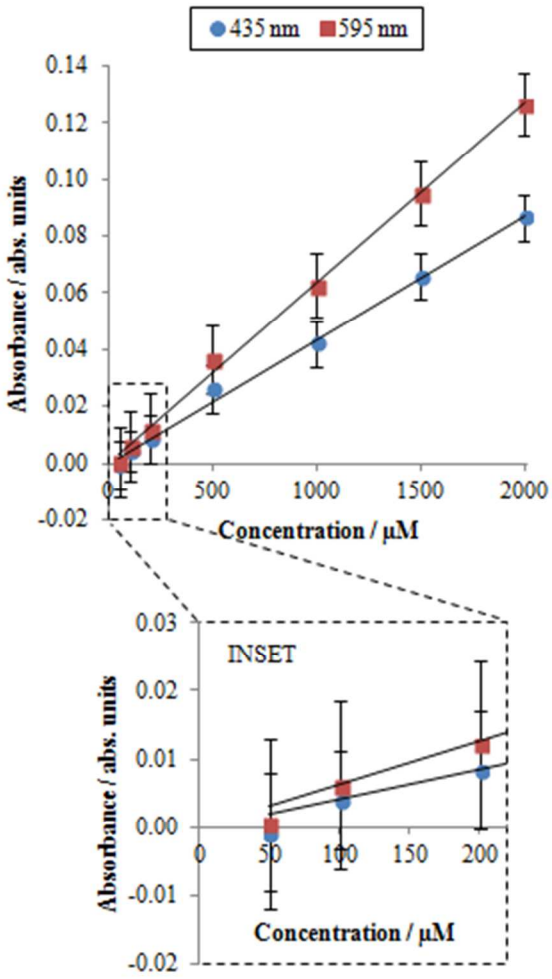

Fig. 5 Single-pass absorbance versus thymol blue concentration, recorded through 50 µm height channel, at the dye absorbance peaks of 435 nm (blue dots) and 595 nm (red squares). 2σ error bars are shown, determined from the noise in 10 acquisitions of I and I_0. The inset shows only the lowest concentrations from 0 – 200 µM.

Compared with the bench-top spectrometer, the on-chip minimum detectable concentration $C_{min,r}$ is approximately 24 times higher at 595 nm. Considering that the absorption path length is, in contrast, approximately 200 times shorter on-chip, this indicates the superior stability of the on-chip optical set-up, which can be seen by comparing $A_{min,r}$ between the two configurations. Excellent agreement is established between the absorption coefficient determined either in the bench-top UV/vis spectrometer or on-chip, at both 435 nm and 595 nm.

3.3 CEAS measurements on-chip

The absorbance of five different concentrations of thymol blue indicator dye in the range 10 – 200 µM was measured on-chip, across the 50 µm height channel with ESRII film. The LED drive current was increased from 150 mA to 700 mA, and the spectrometer integration time was increased from 50 ms to

1000 ms. These changes were necessary to account for the significantly reduced signal levels recorded after the light has passed through two pieces of ESRII film (Fig. 3). Data are presented in Fig. 6, plotted as $I_0/I - 1$ (Eq. 2).

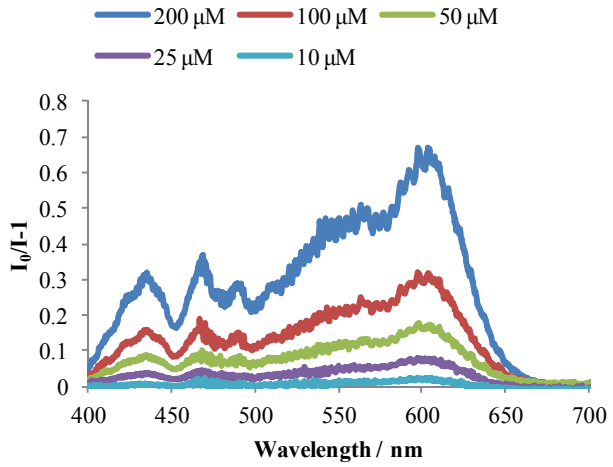

Fig. 6 $I_0/I - 1$ as a function of wavelength, for various concentrations of thymol blue, recorded through 50 µm height channel, with integrated ESRII film. The average of three pairs of recorded I_0/I values is shown for each concentration.

As an example, data for a range of concentrations at the dye peaks of 435 nm and 495 nm were extracted from Fig. 6 and are presented in Fig. 7. Good linearity was observed at both wavelengths, with $R^2 = 0.9916$ at 435 nm and $R^2 = 0.9935$ at 595 nm.

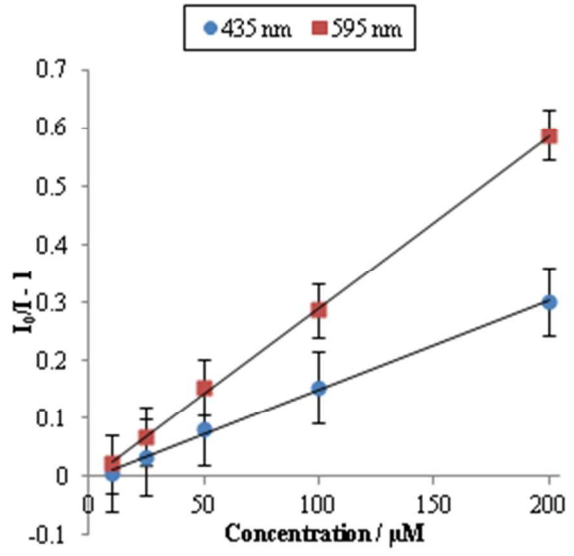

Fig. 7 $I_0/I - 1$ versus thymol blue concentration, recorded through 50 µm height channel with ESRII film, at the dye absorbance peaks of 435 nm (blue dots) and 595 nm (red squares). 2σ error bars are shown, determined from the noise in 10 acquisitions of I and I_0.

From the gradient of the plot shown in Fig. 7, we can calculate the CEF by rearranging Eq. 2, and using the on-chip absorption coefficient at each wavelength presented in Table 2. The CEF at 435 nm was found to be 15, while the CEF at 595 nm was slightly higher, at 20. The minimum absorbance can also be determined from the y-intercept of each plot shown in Fig. 7. The detection limits determined using both the spectral and the regression method are summarised in Table 3, where the spectral method detection limit was determined from the 3σ noise in 50 repeated measurements of I_0 (Tris buffer).

	435 nm	**595 nm**
CEF	15	20
$\mathbf{A_{min,s}}$ **/ a. u.**	4.62×10^{-4}	4.64×10^{-4}
$\mathbf{A_{min,r}}$ **/ a. u.**	3.45×10^{-4}	4.41×10^{-4}
$\boldsymbol{\alpha_{min,s}}$ **/ cm^{-1} Hz$^{-1/2}$**	9.83×10^{-2}	9.88×10^{-2}
$\boldsymbol{\alpha_{min,r}}$ **/ cm^{-1} Hz$^{-1/2}$**	2.32×10^{-1}	2.97×10^{-1}
$\mathbf{C_{min,s}}$ **/ µM Hz$^{-1/2}$**	10.6	7.3
$\mathbf{C_{min,r}}$ **/ µM Hz$^{-1/2}$**	24.9	22.0

Table 3 Detection limits determined on-chip, with ESRII film. 3σ errors are provided for the absorption coefficient, ε.

Integrating ESRII film around the 50 µm height channel has lowered the minimum detectable concentration $C_{min,s}$ by approximately 4.5 times, from 33 µM to 7 µM at 595 nm, and by approximately 5.0 times, from 52.7 µM to 10.6 µM at 435 nm. The on-chip $C_{min,r}$ detection limit of 22 µM at 595 nm with ESRII film is only an order of magnitude higher than the bench-top detection limit of 2 µM obtained at 595 nm, which is particularly impressive when it is considered that the path length is approximately 200 times shorter on-chip.

By rearranging Equation 2, we also can determine the CEF at each wavelength, given the absorbance of the indicator dye determined in Fig. 4, and the measured $(I_0/I) - 1$ values presented in Fig. 6. Example CEF data calculated using 100 µM thymol blue are presented in Fig. 8.

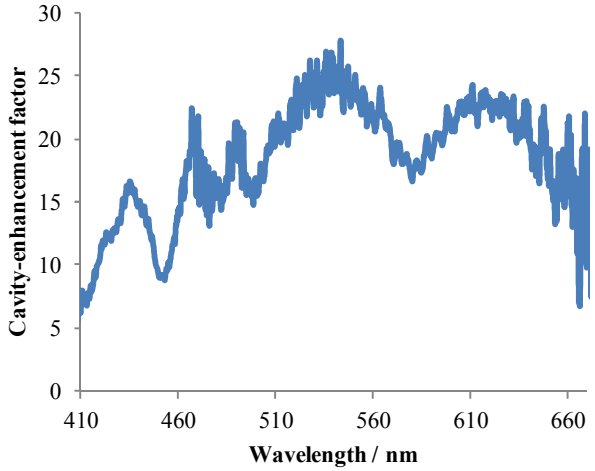

Fig. 8. Cavity-enhancement factor versus wavelength, determined using 100 µM thymol blue absorbance spectra.

The maximum observed CEF is 28 at 544 nm, yielding a total absorption path length at 544 nm of 1.316 mm from a physical path length of 0.047 mm. While the path length has been enhanced by up to 28 times, the sensitivity improvement is noticeably lower, at approximately 5 times. This is a result of the increased noise in the cavity-enhanced experiment, which is limited by the lower light levels compared with the single-pass experiment. The use of a brighter light source or more sensitive detector would enable the cavity-enhanced measurements to be an order of magnitude more sensitive than the single-pass measurements. For example, Neil and coworkers achieved a sensitivity two orders of magnitude higher than this work, at 7.86×10^{-4} cm^{-1} $Hz^{-1/2}$ at 487 nm, using a supercontinuum light source and high sensitivity spectrometer.[8]

The reflectivity can be calculated from the CEF, and is presented as a function of wavelength in Fig. 9.

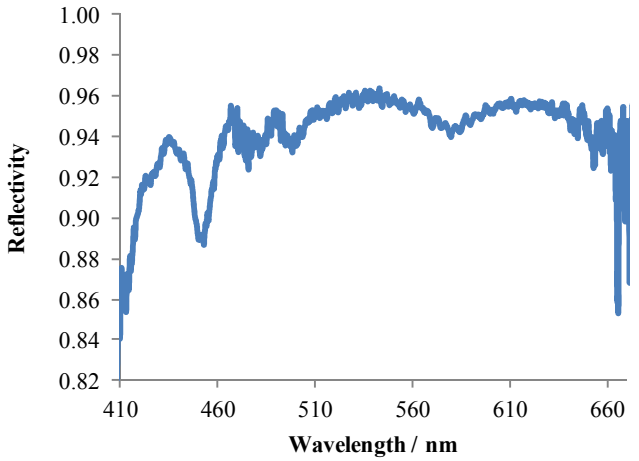

Fig. 9: Reflectivity as a function of wavelength, calculated from the CEF values shown in Fig. 8.

ESRII film has a reported reflectivity of > 98% across 400 – 800 nm. However, placing its surface in contact with PDMS instead of air will lower the reflectivity of ESRII film. The maximum reflectivity of the on-chip cavity, at 544 nm, was calculated to be 96.41%. Note that the decrease in reflectivity observed below 432 nm is a result of the decreasing LED intensity rather than actual reflectivity decrease, while the calculated reflectivity above 660 nm is limited by the dye's low absorbance above 660 nm.

A comparison of the results obtained with ESRII film to those with a similar chip with integrated higher reflectivity dielectric mirrors, would provide an indication of whether the losses are primarily from the ESRII film or the PDMS channel walls.

By integrating the mirrors around a microchannel, we have reduced the cavity length from tens of centimetres, to a few hundred micrometres. This greatly simplifies the LED and detector alignment to the cavity. Additionally, mirror integration within the microfluidic chip reduces the need for extremely high optical quality surfaces on the chip exterior.

The reported $A_{min,s}$ of around 4.6×10^{-4} a. u. lies slightly higher than $0.3 - 1 \times 10^{-4}$ a. u. reported by van der Sneppen and coworkers for a white LED, 99% cavity mirrors and similar spectrometer.[13] In addition, owing to the lower ESRII film reflectivity, the CEF reported in this work is approximately four times lower than the CEF of around 60 achieved by van der Sneppen and coworkers.[13]

It should be noted that the CEFs achievable with a cavity comprised of two pieces of ESRII film are higher than that reported for an alternative type of cavity, which employs a loop of optical fibre.[19] Optical fibre-loops typically suffer from poor CEFs in the range 2 – 12 once a sample region is introduced.[6] In addition, cavity integration around a microchannel is much simpler with ESRII film as no special alignment is required, in contrast to the use of optical fibres, and optical fibre loops in particular, which require the fibre ends to be well-cleaved and carefully aligned with respect to each other.

4. Conclusion

We have described a simple and robust method for integrating ESRII film within a PDMS chip to form a cavity, which allows the absorption path length to be enhanced by an order of magnitude, and the sensitivity to be increased approximately 5-fold, without greatly increasing the experimental cost or complexity. This approach has potential applications for environmental and biological assays in microfluidic formats, facilitating construction of systems capable of measuring relevant compound concentrations.

Acknowledgements

This report represents independent research by the National Institute for Health Research (Invention for Innovation (i4i), Rapid detection of infectious agents at point of triage (PoT), II-ES-0511-21002). The views expressed in this publication are those of the author(s) and not necessarily those of the NHS, the National Institute for Health Research or the Department of Health. The authors would like to thank Hend Alkhammash and Sumit Kalsi for their help with master fabrication, Philip King for photographing the chips, and Lesley Parry-Jones for helpful discussions.

Notes and references

[a] Department of Electronics and Computer Science, University of Southampton, Highfield Campus, Southampton, SO17 1BJ, UK.
[b] Institute of Life Sciences, University of Southampton, Highfield Campus, Southampton, SO17 1BJ, UK.
[c] Sharp Laboratories of Europe, Oxford Science Park, Edmund Halley Road, Oxford, OX4 4GB, UK.
[d] Department of Chemistry, University of Southampton, Highfield Campus, Southampton, SO17 1BJ, UK.

Electronic Supplementary Information (ESI) available: [details of any supplementary information available should be included here]. See DOI: 10.1039/b000000x/

1. V. Srinivasan, V. K. Pamula and R. B. Fair, Anal. Chim. Acta, 2004, **507**, 145.
2. M. H. Wu, H. Cai, X. Xu, J. P. G. Urban, Z.-F. Cui and Z. Cui, Biomed. Devices, 2005, **7**, 323.
3. J. V. Sieben, C. F. A. Floquet, I. R. G. Ogilvie, M. C. Mowlem and H. Morgan, Anal. Methods, 2010, **2**, 484.
4. C. F. A. Floquet, V. J. Sieben, A. Milani, E. P. Joly, I. R. G. Ogilvie, H. Morgan and M. Mowlem, Talanta, 2011, **84**, 235.
5. L. van der Sneppen, F. Ariese, C. Gooijer and W. Ubachs, Annu. Rev. Anal. Chem., 2009, **2**, 13.
6. C. M. Rushworth, J. Davies, J. T. Cabral, P. R. Dolan, J. M. Smith and C. Vallance, Chem Phys Lett, 2012, **554**, 1.
7. M. Mazurenka, A. J. Orr-Ewing, R. Peverall and G. A. D. Ritchie, Ann. Rep. Prog. Chem., Sect. C, 2005, **101**, 100.
8. S. R. T. Neil, C. M. Rushworth, C. Vallance and S. R. Mackenzie, Lab Chip, 2011, **11**, 3953.
9. S. M. Ball, J. M. Langridge and R. L. Jones, Chem. Phys. Lett., 2004, **398**, 68.
10. M. Islam, N. Seetohul and Z. Ali, Appl. Spectrosc., 2007, **61**, 649.
11. N. Seetohul, Z. Ali and M. Islam, Analyst, 2009, **134**, 1887.
12. N. Seetohul, Z. Ali and M. Islam, Anal. Chem., 2009, **81**, 4106.
13. L. van der Sneppen, G. Hancock, C. Kaminski, T. Laurila, S. R. Mackenzie, S. R. T. Neil, R. Peverall, G. A. D. Ritchie, M. Schnippering and P. R. Unwin, Analyst, 2010, **135**, 133.
14. L. Billot, A. Plecis and Y. Chen, Microelectron. Eng., 2008, **85**, 1269.
15. A. J. C. Kuehne, M. C. Gather, I. A. Eydelnant, S.-H. Yun, D. A. Weitz and A. R. Wheeler, Lab Chip, 2011, **11**, 3716.
16. US Pat., US5882774A, 1999.
17. H. Zhang and R. H. Byrne, Mar. Chem., 1996, **52**, 17.
18. V. M. C. Rérolle, C. F. A. Floquet, A. J. K. Harris, M. C. Mowlem, R. R. G. J. Bellerby and E. P. Achterberg, Anal. Chim. Acta, 2013, **786**, 124.
19. R. S. Brown, I. Kozin, Z. Tong, R. D. Oleschuk and H.-P. Loock, J. Chem. Phys., 2002, **117**, 10444.

